

EIGHTEENTH EUROPEAN ROTORCRAFT FORUM

E . 08

PAPER N 21

INVESTIGATIONS OF HELICOPTER TAIL ROTOR
LOADING IN HOVERING TURNS

M.G. ROZHDESTVENSKY

September 15-18, 1992

AVIGNON, FRANCE

ASSOCIATION AERONAUTIQUE ET ASTRONAUTIQUE DE FRANCE

INVESTIGATIONS OF HELICOPTER TAIL ROTOR LOADING IN HOVERING TURNS

M.G. Rozhdestvensky
Mil Moscow Helicopter Plant, Russia

The paper describes the method used for investigations of the tail rotor blade loads in hovering and the results obtained. The developed analytical method is specific as its single algorithm covers all known types of blade-to-head attachments, and, when analysing loads, the tail rotor as a whole is considered. This allows to determine loads applied to gimbaled rotors, two-bladed teetering rotors and their combinations in the form of four-bladed rotors consisting of two pairs of two-bladed teetering rotors with due account of attachment elastic properties of each two-bladed module.

SUBJECT OF INVESTIGATIONS. COORDINATE SYSTEMS

The helicopter making a turn in the horizontal plane relative to the centre of gravity position in hovering is investigated. The helicopter rotates at an angular velocity, $\bar{\Omega}$, and with an angular acceleration $\dot{\bar{\Omega}}$. The tail rotor rotates steadily at an angular velocity $\bar{\omega}$. The following counterclockwise coordinate systems are introduced (Figure 1):

- $O_3 X_3 Y_3 Z_3$ fixed earth axes;
- $O_B X_B Y_B Z_B$ helicopter centre of mass coordinate system; the X_B axis runs in the flight direction, and the Y_B axis, along the main rotor shaft;
- $O_1 X_1 Y_1 Z_1$, tail rotor head coordinate system; the Z_1 axis runs along the tail rotor shaft, the Y_1 axis, along the projection of one of the head sleeves on the plane of rotation.

The triads of the single vectors \bar{e}_3, \bar{e}_B and \bar{e}_1 are connected with the centre of each system.

The matrix of transition from the earth axes to the helicopter axes is:

$$C_{B_3} = \begin{pmatrix} \cos\theta & 0 & -\sin\theta \\ 0 & 1 & 0 \\ \sin\theta & 0 & \cos\theta \end{pmatrix}. \quad (1)$$

The matrix of transition from the helicopter axes to the tail rotor axes is:

$$C_{1_B} = \begin{pmatrix} \cos\psi & \sin\psi & 0 \\ -\sin\psi & \cos\psi & 0 \\ 0 & 0 & 1 \end{pmatrix}. \quad (2)$$

BLADE ELEMENT VELOCITIES

The radius-vector of a blade point is:

$$\bar{r}_a = \bar{r}_3 + \bar{r}_B - \bar{r}_1. \quad (3)$$

The absolute velocity of a blade point is an absolute time derivative of the radius-vector of this particular point:

$$\bar{v}_a = \frac{d\bar{r}_a}{dt} = \frac{d\bar{r}_3}{dt} - \frac{d\bar{r}_B}{dt} + \frac{d\bar{r}_1}{dt}. \quad (4)$$

The first term in this expression is the velocity of the helicopter centre of mass, the second, the velocity of the tail rotor hub centre, and the third, the velocity of the relative blade section movement.

With $\frac{d\vec{r}_3}{dt} = \vec{v}_B$; $\frac{d\vec{r}_B}{dt} = \vec{\Omega} \times \vec{r}_B$; $\frac{d\vec{r}_1}{dt} = \vec{v}_r - (\vec{\omega} - \vec{\Omega}) \times \vec{r}_1$, and, using the transition matrices C_{0_3} and C_{1_8} to change over to the triad axes \vec{e}_1 , we can obtain projections of the absolute velocity of the blade points.

$$\vec{v}_a = \vec{e}_1 \begin{pmatrix} l_{X_1} \\ l_{Y_1} \\ l_{Z_1} \end{pmatrix} = \vec{e}_1 \begin{pmatrix} \cos\psi(\cos\theta l_{X_B} - l_{Z_B} \sin\theta) - \Omega l_{K_0} \cos\psi - \dot{r}_{X_1} - \omega r_{Y_1} + \Omega r_{Z_1} \cos\psi \\ -\sin\psi(\cos\theta l_{X_B} - l_{Z_B} \sin\theta) - \Omega l_{K_0} \sin\psi - \dot{r}_{Y_1} + \omega r_{X_1} - \Omega r_{Z_1} \sin\psi \\ \sin\theta l_{X_B} + l_{Z_B} \cos\theta - \Omega l_{X_0} - \dot{r}_{Z_1} - \Omega r_{X_1} \cos\psi - \Omega r_{Y_1} \sin\psi \end{pmatrix} \quad (5)$$

AIR FLOW VELOCITIES IN BLADE SECTIONS

Let us place the $O_i X_i Y_i Z_i$ counterclockwise coordinate system in some i -th blade section so that the X_i -axis could run along the blade chord towards the trailing edge, and the Y_i -axis, at a tangent to the blade rigid axis of this section, and the Z_i -axis, normal to the $O_i X_i Y_i$ plane (Figure 2).

During blade deformation, each section turns by an angle β_y in the $Z_i O_i Y_i$ plane of thrust, and by an angle β_x in the $X_i O_i Y_i$ plane of rotation.

We can get the C_{i_1} transition matrix from the $O_i X_i Y_i Z_i$ coordinate system having the \vec{e}_1 triad to the $O_i X_i Y_i Z_i$ coordinate system by assuming that the angles β_x and β_y are small:

$$C_{i_1} = \begin{pmatrix} 1 & -\beta_y & 0 \\ \beta_x & 1 & \beta_y \\ 0 & -\beta_x & 1 \end{pmatrix}. \quad (6)$$

The β_y angle comprises the a_{0_k} design coning angle if it is available in the rotor, i.e.

$$\beta_y = a_{0_k} - \beta_y^*, \quad (7)$$

where β_y^* is the elastic component of the blade section angle in the plane of thrust.

Having the air flow velocity projections in the \vec{e}_1 triad axes that are equal in magnitude but opposite in sign to expressions (5), and the C_{i_1} transition matrix from the \vec{e}_1 triads connected to the rotor centre to the \vec{e}_i triad axes, we can get air flow velocity projections in each blade section with due account of its deformation in two planes:

$$\vec{V} = \vec{e}_i C_{i_1} \begin{pmatrix} -V_{X_1} \\ -V_{Y_1} \\ -V_{Z_1} \end{pmatrix} = \vec{e}_i \begin{pmatrix} -V_{X_1} + \beta_x V_{Y_1} \\ -\beta_x V_{X_1} - V_{Y_1} - \beta_y V_{Z_1} \\ \beta_y V_{Y_1} - V_{Z_1} \end{pmatrix} \quad (8)$$

TAIL ROTOR INDUCED VELOCITIES

The calculation of tail rotor induced velocities in hovering turns is made by using the vortex theory [1] which allows to take into account radial and azimuth variability of the air flow velocity normal to the rotor disc that occurs in hovering turns. The initial equations used for calculations of induced velocities are the following:

- equation used for calculation of the circulation at each disc point

$$\Gamma(\bar{r}, \psi) = \frac{1}{2} C_Y(\bar{r}, \psi) U_x b; \quad (9)$$

- equation used for calculation of the circulation distributed along the blade radius

$$\gamma(\bar{r}, \psi) = \frac{Z \Gamma(\bar{r}, \psi) U_x}{2 \cdot \pi \cdot r (V_0 + v_1)}. \quad (10)$$

In the axial flow condition

$$\gamma(\bar{r}, \psi) = 2v_1(\bar{r}, \psi). \quad (11)$$

Using equations (9) and (10) with due account of equation (11), we can get the equation required to calculate the induced velocity at each point of the rotor disc.

$$v_1(\bar{r}, \psi) = -\frac{V_0}{2} + \sqrt{\frac{V_0^2}{4} + \frac{C_Y(\bar{r}, \psi) \sigma \cdot r}{8}}. \quad (12)$$

This equation coincides with that used in the momentum transfer theory to calculate the induced velocity, but here V_0 denotes the magnitude of the air flow speed at each point of the rotor:

$$V_0 = -\Omega l_{x_0} - \Omega r_y \sin \psi.$$

In making turns where the tail rotor operates in the conditions similar to that of the main rotor in vertical descent, the magnitude of the induced velocity should be corrected with due account of the induced velocity value dependence of the helicopter rate of descent based on experimental data [2, 3]. This dependence reflects changes in the rotor disc air flow pattern in conditions of the vortex ring, as well as those close to it. The values of the induced velocity in this paper are corrected for the value of the axial velocity V_0 corresponding to the tail rotor disc centre.

ACCELERATION OF BLADE ELEMENTS

Equations expressing the projections of absolute blade element accelerations required for calculation of inertia loading have been obtained as time derivatives of the absolute blade section velocity

$$\bar{u}_a = \frac{d\bar{V}_a}{dt} = \frac{d}{dt} (\bar{V}_3 + \bar{V}_0 + \bar{V}_1 + (\bar{\omega} + \bar{\Omega}) \times \bar{r}). \quad (13)$$

and they take the form:

$$\begin{aligned} w_{a_{x_1}} &= -2\omega \dot{r}_{y_1} + \frac{1}{2} \Omega^2 [r_{y_1} \sin 2\psi - r_{x_1} (1 + \cos 2\psi)] + [\epsilon_\Omega (l_{k_0} \delta + r_{z_1}) + \Omega^2 l_{x_0} \delta + 2\Omega r_{z_1}] \cos \psi, \\ w_{a_{y_1}} &= -\frac{1}{2} \Omega^2 r_{y_1} + 2\omega \dot{r}_{x_1} - [\epsilon_\Omega (l_{k_0} \delta + r_{z_1}) + \Omega^2 l_{k_0} \delta + 2\Omega r_{z_1}] \sin \psi + \frac{1}{2} \Omega^2 r_{x_1} \sin 2\psi + \frac{1}{2} \Omega^2 r_{y_1} \cos 2\psi, \\ w_{a_{z_1}} &= \epsilon_\Omega l_{x_0} \delta - \Omega^2 (l_{k_0} \delta + r_{z_1}) + [-\epsilon_\Omega r_{x_1} + 2\Omega (\omega r_{y_1} - \dot{r}_{x_1})] \cos \psi + [\epsilon_\Omega r_{y_1} + 2\Omega (\omega r_{x_1} + \dot{r}_{y_1})] \sin \psi. \end{aligned} \quad (14)$$

EFFECT OF TAIL ROTOR DRIVE SHAFT VIBRATION ON
BLADE LOADS

The tail rotor loading is scarcely affected by the tail rotor drive shaft vibration. However, when some frequency of the tail rotor drive shaft end is close to a frequency of the tail rotor blades the level of the loads is naturally expected to rise. Thus, for example, a significant tail rotor loading dependence of the tail rotor gearbox vibration level equal to the 9 per main rotor revolution frequency has been registered for the Mi-2 tail rotor.

To evaluate this phenomenon, it is necessary to add the projections of the vibrational acceleration vector of the tail rotor drive shaft end to the like projections of the absolute acceleration vector:

$$\vec{u}_p = \vec{e}_i \begin{pmatrix} u_{y_p} \sin \psi \\ u_{y_p} \cos \psi \\ u_{z_p} \end{pmatrix} \quad (15)$$

Vibrations of the tail rotor drive shaft end occur at several frequencies, therefore, the vibrational acceleration values are determined as a sum of the vibrational accelerations occurring at each frequency.

METHOD USED TO CALCULATE BLADE NATURAL OSCILLATION
FREQUENCIES AND MODES

To determine frequencies and modes of twisted blade natural oscillations, use is made of the calculational technique [4] which has been obtained from the familiar three-moment method applied for the first time by T. Morris and W. Tye to compute forced oscillations of the blade in one plane in the centrifugal field. The calculated modes of the blade lateral oscillations are characterized by displacements in two mutually perpendicular directions which, in their turn, are perpendicular to the blade longitudinal line. These directions coincide with the rotor planes of rotation and thrust, moreover, bending moments corresponding to each mode of natural oscillations are determined for the same directions. Boundary conditions characterizing the blade-to-hub attachment type can be different for the plane of rotation and that of thrust thus allowing to define the frequencies and modes of blade oscillations for different combinations of hub attachment conditions, and the way the initial data are specified allows to describe rather accurately the mass and flexural rigidity distribution along the blade radius.

APPLICATION OF THE BUBNOV-GALERKIN METHOD TO SOLVE
THE PROBLEM

Blade motion under external loads is determined by the Bubnov-Galerkin method; to do this, coupled blade natural flexural oscillation modes in the planes of rotation and thrust are used. The oscillation modes are considered to be vector-functions of the blade radius with two components X and Z:

$$U_i(r_j, t) = \{z_i(r), x_i(r)\} \delta_i(t). \quad (16)$$

As a rule, when the Bubnov-Galerkin method is used to solve equations expressing coupled oscillations, a system of related differential equations as to the unknown time functions $\delta_i(t)$ is obtained:

$$\delta_i + p_i^2 \delta_i = \frac{1}{m_{np_i}} \int_0^R [L_z \cdot Z_i(r) + L_x \cdot X_i(r)] dr; \quad i = 1, 2, \dots, n. \quad (17)$$

Here, p_i - is the frequency of the i -th mode of the blade oscillations
 m_{np_i} - is the reduced mass of the i -th mode of the blade oscillations
 L_z - is the blade external load in the plane of rotor thrust
 L_x - is the blade external load in the plane of rotation

This approach allows to calculate motion of an isolated blade and its stresses.

However, there exist types of rotors for which it is impossible to compute blade stresses by using this method. These are: two-bladed teetering rotors, three-bladed gimbaled rotors and four-bladed rotors consisting of two pairs of two-bladed teetering rotors with due account of the attachment elastic properties of each two-bladed module.

The difficulty is that even and odd excitation harmonics result in oscillations of blades having different types of blade-to-hub attachment. For example, in the two-bladed teetering rotor odd excitation harmonics make the blades oscillate flapwise as if they were articulated, and chordwise as if they were rigidly fixed; whereas even excitation harmonics make the blades oscillate chordwise as if they were rigidly fixed, and flapwise as if they were articulated. But it should be borne in mind that the in-plane articulated blade is rather conventional as the tail rotor drive shaft torsional stiffness is not equal to zero. To determine blade load constant components, it is necessary to consider a third type of blade-to-hub attachment type, i.e. chordwise and flapwise rigidly fixed blade root.

The above mentioned problem can be solved by introducing rotor oscillation modes. The notion about normal modes of the elastic blade motion has been introduced by L.N. Grodko [5].

Figures 3, 4 and 5 show normal oscillation modes of two-, three- and four-bladed rotors. Blade motion in the K -th rotor oscillation mode can be presented by the N_K natural oscillation modes of the blade with the appropriate conditions of the hub attachment. Blade deformation with due account of motion in all normal modes can be calculated by using the following equations:

- in the thrust plane

$$Z(r, t) = \sum_{K=1}^{N_K} \sum_{j=1}^{n_T} \delta_K^j(t) Z^j(r); \quad (18)$$

- in the plane of rotation

$$X(r, t) = \sum_{K=1}^{N_K} \sum_{j=1}^{n_T} \delta_K^j(t) X^j(r).$$

Here, K - is the number of normal rotor oscillation mode;
 j - is the number of the natural oscillation overtone of an isolated blade;
 δ_K^j - is a coefficient of blade deformation in respect to the j th overtone of K -th rotor oscillation mode.

Due to the introduction of the rotor oscillation modes, the system of equations used for calculating deformation coefficients by the Bubnov-Galerkin method will take the form

$$\delta_K^j + p_{K_j}^2 \delta_K^j = \frac{1}{m_{np_K}} \sum_{i=1}^{n_B} \int_0^R (L_z Z_{i_K}^j + L_x X_{i_K}^j) dr; \quad j = 1, 2, \dots, n_T, K = 1, 2, \dots, N_K \quad (19)$$

Here, N_k - is the number of normal rotor oscillation modes;
 n_T - is the number of natural oscillation overtones being considered;
 i - is the rotor blade number;
 n_B - is the number of rotor blades.

Having found the time functions ϵ_k^j tail rotor blade bending moments are obtained

$$M_z(r,t) = \sum_{k=1}^{N_k} \sum_{j=1}^{n_T} \epsilon_k^j(t) \cdot M_z^j(r);$$

$$M_x(r,t) = \sum_{k=1}^{N_k} \sum_{j=1}^{n_T} \epsilon_k^j(t) \cdot M_x^j(r).$$

(20)

And now let us consider expressions for the loads L_z and L_x in equations (17) and (19).

The aerodynamic loads distributed along the blade radius are defined from the known values of the blade section air flow velocity projections (8) with account of the airfoil aerodynamic characteristics.

The inertia components of the in-plane and out-of-plane loads are determined by expressions (14). However, if the tail rotor blades are rigidly attached to the hub with a design coning angle, the acceleration projection (14) gives rise to additional blade out-of-plane loads. For rotors having the design coning angle in the thrust plane in expressions (14), the following sum should be taken for the projection of the vector \vec{r} onto the axis $Z_1 - r_{z_1}$:

$$r_{z_1} = r_{z_1}^* - a_{oK} r,$$

where $r_{z_1}^*$ - is the projection caused by blade deformation;

$a_{oK} r$ - is the elevation of the blade point at r over the plane of rotation caused by the design coning angle.

Let us consider the projection of the absolute acceleration $w_{a_{y_1}}$:

$$w_{a_{y_1}} = -\omega^2 r_{y_1} - \frac{1}{2} \Omega^2 r_{y_1} + 2\omega \dot{r}_{x_1} - [\epsilon_{\Omega} (l_{K\delta} - r_{z_1}) + \Omega^2 l_{K\delta} + 2\Omega \dot{r}_{z_1}] \sin \psi - \frac{1}{2} \Omega^2 r_{x_1} \sin 2\psi + \frac{1}{2} \Omega^2 r_{y_1} \cos 2\psi.$$

The first term is a centripetal acceleration. When the design coning angle is available, it produces time constant blade loads in the thrust plane. Other terms in the expression $w_{a_{y_1}}$ can be considered as a variable component of a centripetal acceleration field that will be an external inertia load.

Let us denote the magnitude of the variable component force N_w :

$$N_w = \int_r^R \left(\frac{1}{2} \Omega^2 r_{y_1} - 2\omega \dot{r}_{x_1} + [\epsilon_{\Omega} (l_{K\delta} - r_{z_1}) + \Omega^2 l_{K\delta} + 2\Omega \dot{r}_{z_1}] \sin \psi - \frac{1}{2} \Omega^2 r_{x_1} \sin 2\psi - \frac{1}{2} \Omega^2 r_{y_1} \cos 2\psi \right) dr.$$

(21)

The final expressions for additional shearing forces caused by the design coning angle as well as by the in-plane and out-of-plane deflections take the form:

$$q_{z_1} = -\pi \omega^2 r_{y_1} a_{oK} - (V_w(z' + a_{oK}))',$$

$$q_{x_1} = -(V_w x')'.$$

(22)

Here z' and x' are in-plane and out-of-plane blade section angles. Since the tail rotor is in the vertical plane the blade weight causes blade loading with in-plane 1 per revolution frequencies.

The shearing forces distributed along the radius are:

$$\begin{aligned} & - \text{in-plane, } q_{x_1} = -mg \sin \psi; \\ & - \text{out-of-plane, } q_{z_1} = mg \cos \psi \sin(c_{\alpha_K} + z'). \end{aligned} \quad (23)$$

Thus, expressions for calculating external loads applied to the blade, take the form:

$$\begin{aligned} L_{z_1} &= \frac{dT}{dr} - m\omega^2 a_{z_1} - m\omega^2 r_{y_1} a_{\alpha_K} - [N_w(z' + \alpha_{\alpha_K})]' + mg \cos \psi \sin(z' + \alpha_{\alpha_K}), \\ L_{x_1} &= \frac{dQ}{dr} - m\omega^2 a_{x_1} - mg \sin \psi - [N_w x']'. \end{aligned} \quad (24)$$

CALCULATED STRESSES IN TAIL ROTOR BLADES IN HOVERING TURNS

When calculating loading, the helicopter turns in hovering are performed by changing the tail rotor pitch from its trim by a specified value and at a specified rate. Typical time variation of the tail rotor pitch is given in Figure 6.

The blade loads and flapping were calculated both for the left- and right-hand turns. In left-hand hovering turns made by the helicopter by reducing the tail rotor pitch from its trim the loads obtained are higher than those obtained in right-hand turns. This is attributed by the fact that in left-hand turns the helicopter angular velocity of rotation already attained is reduced by increasing the tail rotor pitch to the maximum value, and, at the same time, the air flow along the tail rotor axis caused by the helicopter angular velocity of rotation increases still further the blade section angles of attack up to stall values.

Figures 7, 8 and 9 show calculated bending moments and flapping motion amplitudes for the Mi-8 three-bladed gimballed tail rotor at different angular velocities of rotation reached during turns. As can be seen from the figures, the calculated points are within the field of scatter of data obtained in test measurements, and the maximum values of the bending moments and flapping motion amplitudes are close to the maximum values obtained in tests.

Figure 10 shows calculated bending moments in the blade root versus time of turn. Here one can see time variations of the blade flapping motion, helicopter angular velocity, angular acceleration and turn angles. The distribution of the total loads in the planes of maximum and minimum rigidity as well as their components for 3 harmonics along the blade radius are given.

The presented calculation data show that the maximum blade bending moments act with the 1 per revolution frequency. At the same time it can be clearly seen that the component of the moment acting with the 2 per revolution frequency in the total value of the bending moment changes with the tail rotor pitch. The maximum values of the loads applied to the tail rotor during a turn are reached only when the pitch increases from the minimum value to the maximum one. The maximum values of the blade flapping are attained during the same period of time.

The Mi-28 tail rotor is two pairs of two-bladed teetering rotors connected by an elastic member. The elastic member stiffness was chosen so that it could provide the required blade frequency in the lowest skew-symmetric rotor oscillation mode.

The two-bladed modules are arranged so that the minimum angle between the two pairs of blades in the plane of rotation is 36 degrees. This feature makes it impossible to use the pattern of the four-bladed normal modes given in Figure 5, as the pattern is effective for the rotor whose axial symmetry is characterized by the 90-degree rotor angle.

The axial symmetry of the X-form rotor features the 180-degree rotor angle, i.e. it is similar to that of the two-bladed rotor. The pattern of the X-form rotor normal modes assumed in the paper is presented in Figure 11. It is easy to see that the condition of orthogonality is observed for this pattern of normal modes.

To determine the effect of mutual azimuthal location of two pairs of blades on the tail rotor loading, a number of calculations in which the angle between the blade pairs changed from 0 to 90 degrees have been made. Figures 12 and 13 show calculations in the form of dependences of bending moments in the 1st and 2nd harmonics on the angle between two pairs of blades. The parameter ψ_a most significantly affects the in-plane bending moment acting with a 2 per revolution frequency. When the angle changes from 90 degrees to 0, the amplitude value becomes almost 4 times lower. But the value of the total bending moment amplitude changes only by 20%. This is attributed by the fact that the blade loading occurs mainly in the 1st harmonic, the component of the bending moment in the 2nd harmonic in the total value of the bending moment being 33% and 10% for $\psi_a = 90$ degrees and 0 respectively.

Figures 14 and 15 compare the in-plane and out-of-plane bending moment values obtained for the Mi-24 X-form tail rotor in calculations and in tests.

As can be seen from the presented data, the calculated values of the in-plane bending moments show a good agreement with those measured in flights. The out-of-plane bending moment values measured in tests were higher than the calculated ones. It is explained by the fact that, as the test have shown, a significant part of the blade out-of-plane bending moment is made up by the moment acting with a 4 per revolution frequency, which, in its turn, is attributable to the proximity of the blade frequencies to the 4th harmonic resonance. The calculations have not taken into account the 4th harmonic excitation, as a result, the level of calculated loads was almost twice as low as that obtained in flight tests.

CONCLUSIONS

1. A method for calculating blade loading in gimballed, two-bladed teetering tail rotors and their combinations in hovering turns by using normal rotor oscillation modes has been developed.

2. A good agreement of calculated loads and flapping motion amplitudes with flight test results for the Mi-2, Mi-8 and Mi-24 tail rotors has been obtained.

3. The Mi-28 X-form tail rotor loading has been investigated, and a significant effect of the azimuth angle between two pairs of blades on the 2 per revolution bending moment amplitude has been shown.

REFERENCES

1. Шайдаков В.И. Обобщенная дисковая вихревая теория и методы расчета индуктивных скоростей несущего винта вертолета. В кн.: Проектирование вертолетов. Вып. 406. МАИ, 1977.

2. Акимов А.И. Аэродинамика и летные характеристики вертолетов. М. Машиностроение, 1988.

3. Джонсон У. Теория вертолета. М., "МИР", 1983.

4. Шнуров З.Е. Метод конечного элемента с итерациями для расчета формы частот свободных колебаний естественно закрученных лопастей воздушных винтов. Труды ЦАГИ, вып. 1430.

5. Гродко Л.Н. Задачи о связанных колебаниях лопастей несущего винта. Технический отчет МВЗ, N 2. М., 1967.

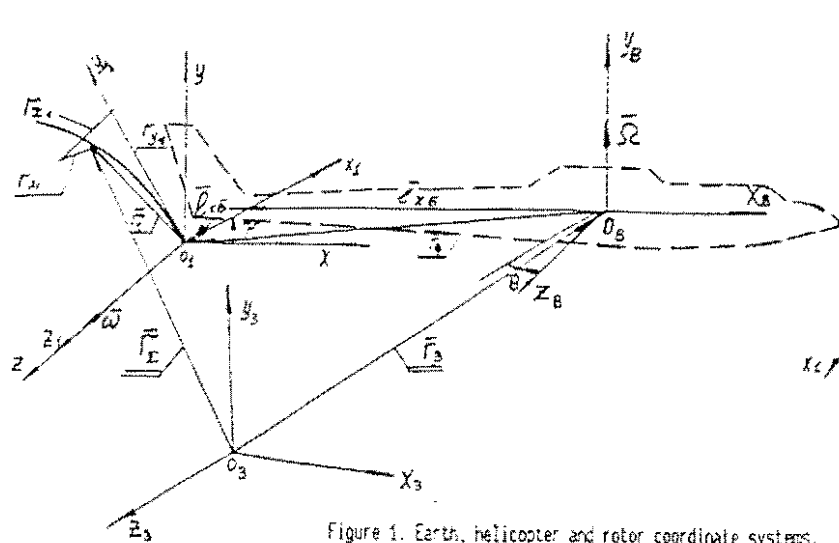


Figure 1. Earth, helicopter and rotor coordinate systems.

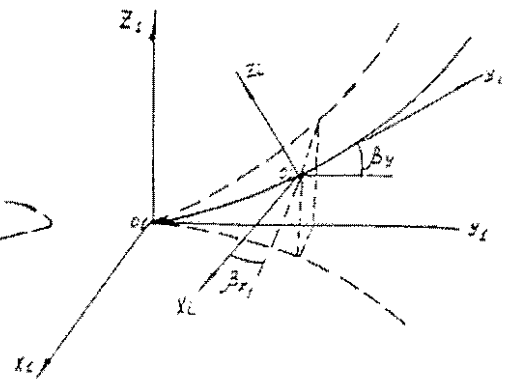


Figure 2. Blade coordinate system.

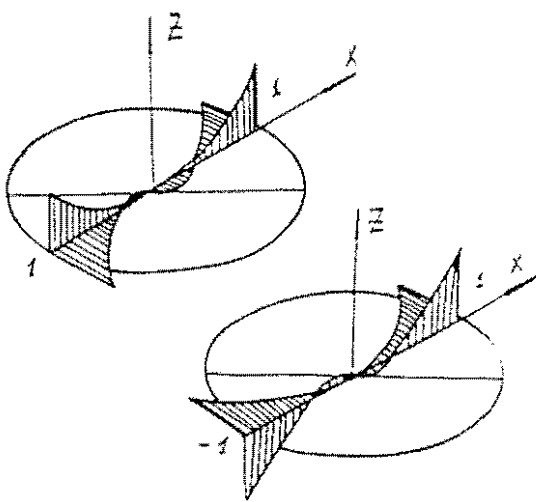


Figure 3. Normal oscillation modes of a two-bladed teetering rotor.

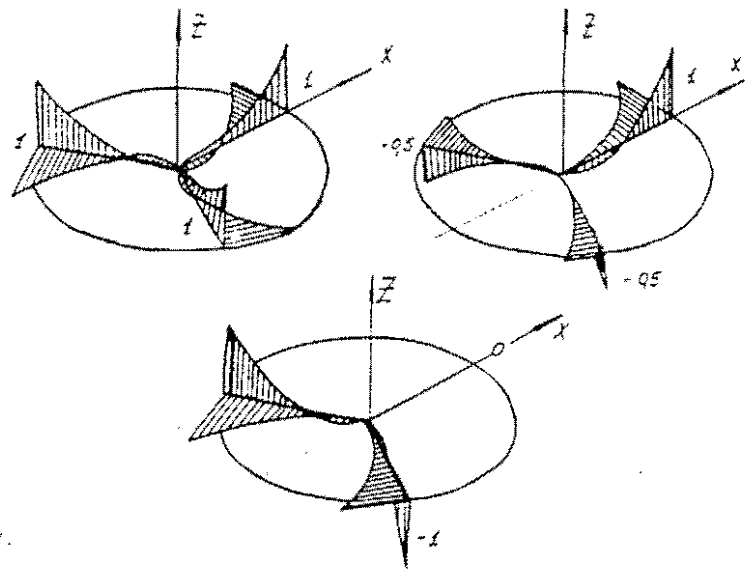


Figure 4. Normal oscillation modes of a three-bladed gimballed rotor.

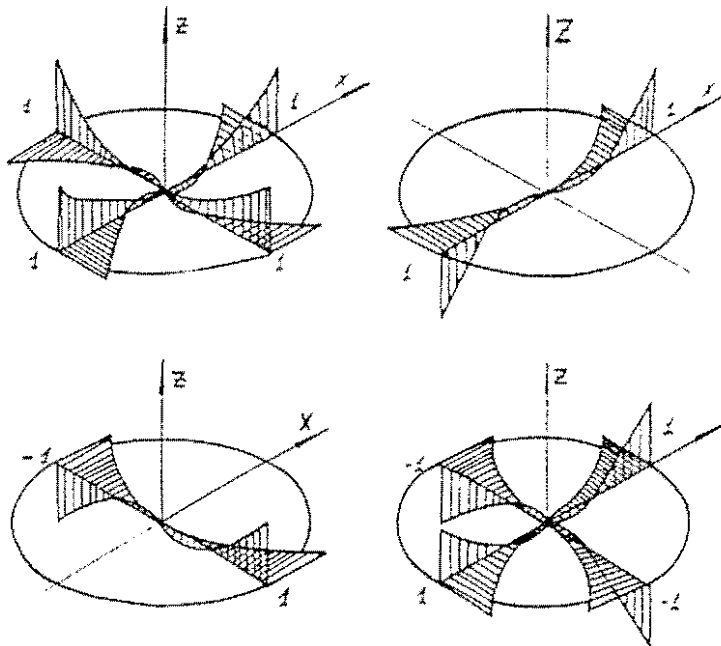


Figure 5. Normal oscillation modes of a four-bladed rotor incorporating flapping hinges.

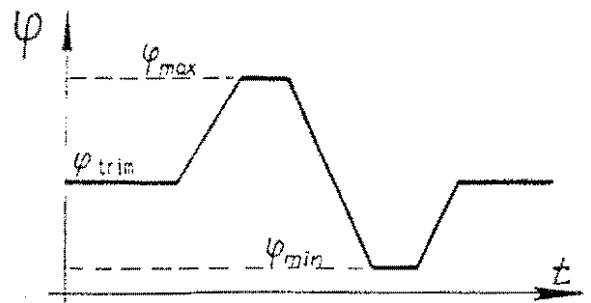


Figure 6. Typical time variation of pitch change.

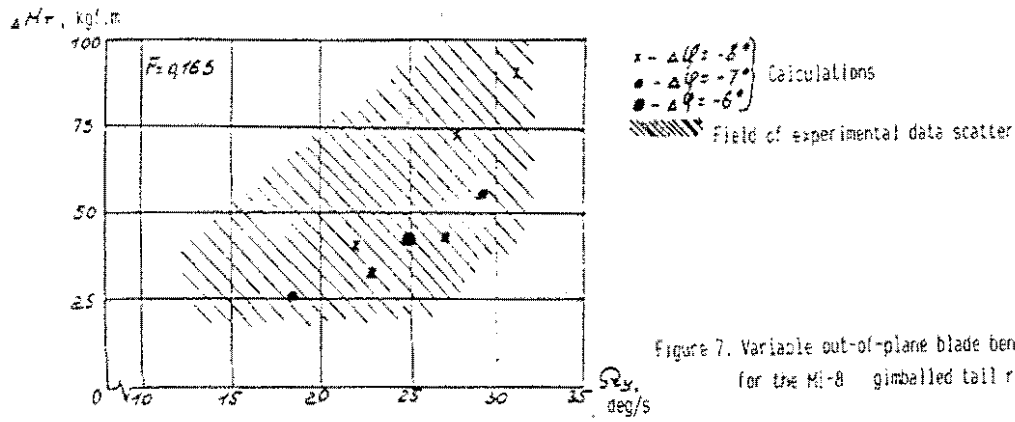


Figure 7. Variable out-of-plane blade bending moment for the Mi-8 gimbal tail rotor.

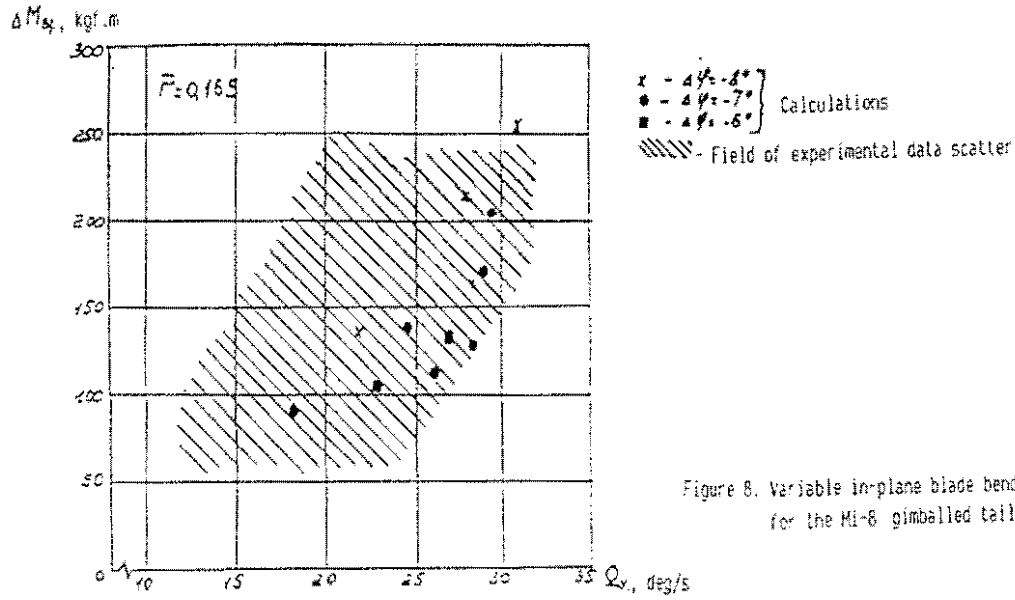


Figure 8. Variable in-plane blade bending moment for the Mi-8 gimbal tail rotor.

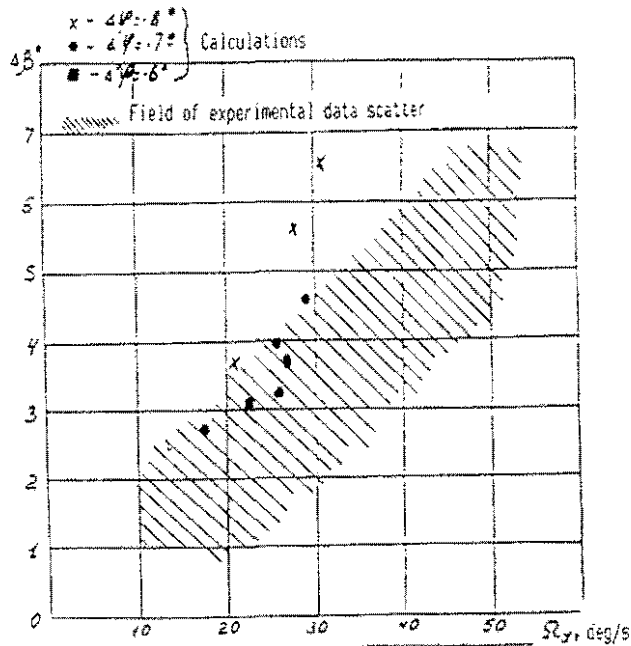


Figure 9. Amplitude of blade flapping motion for the Mi-8 and Mi-24 gimbal tail rotors.

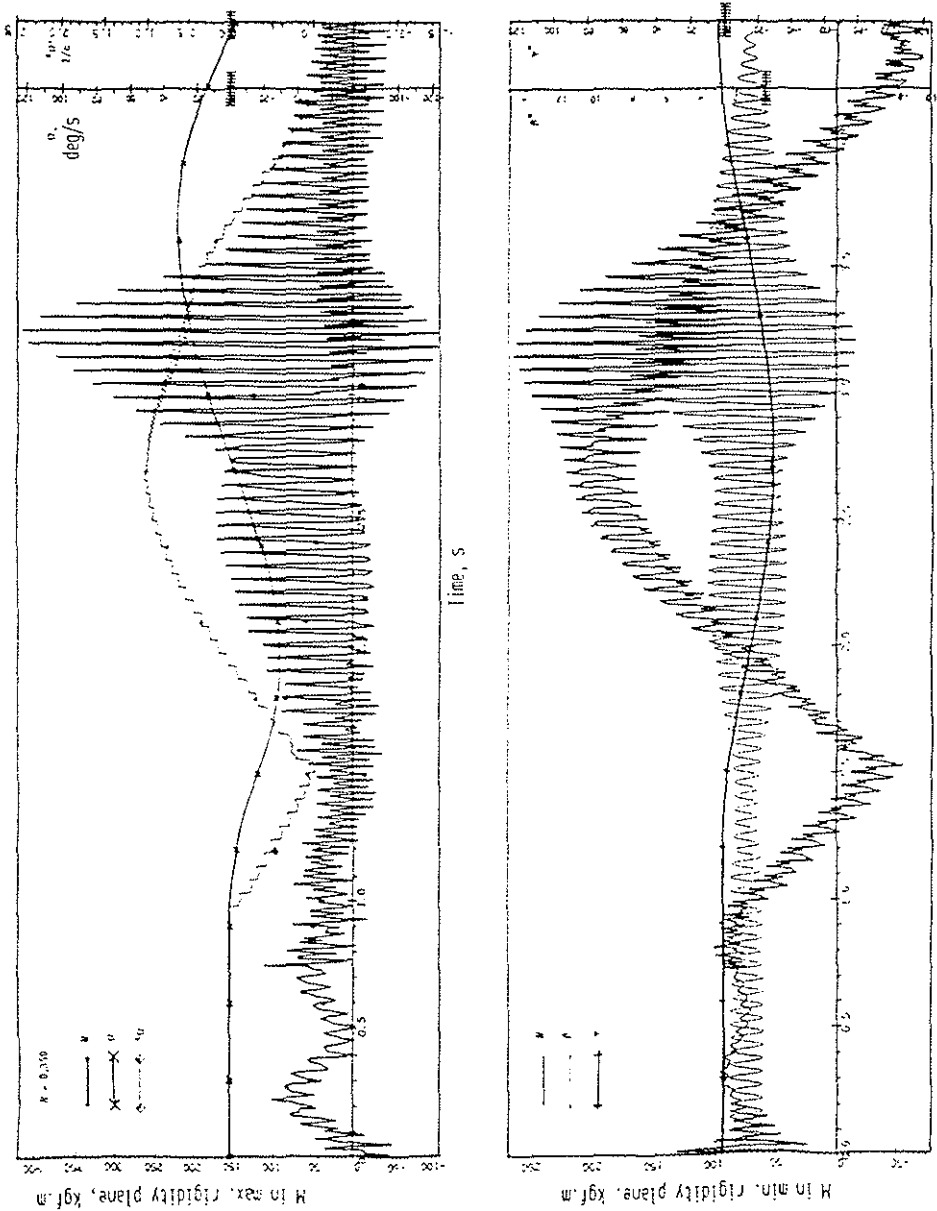
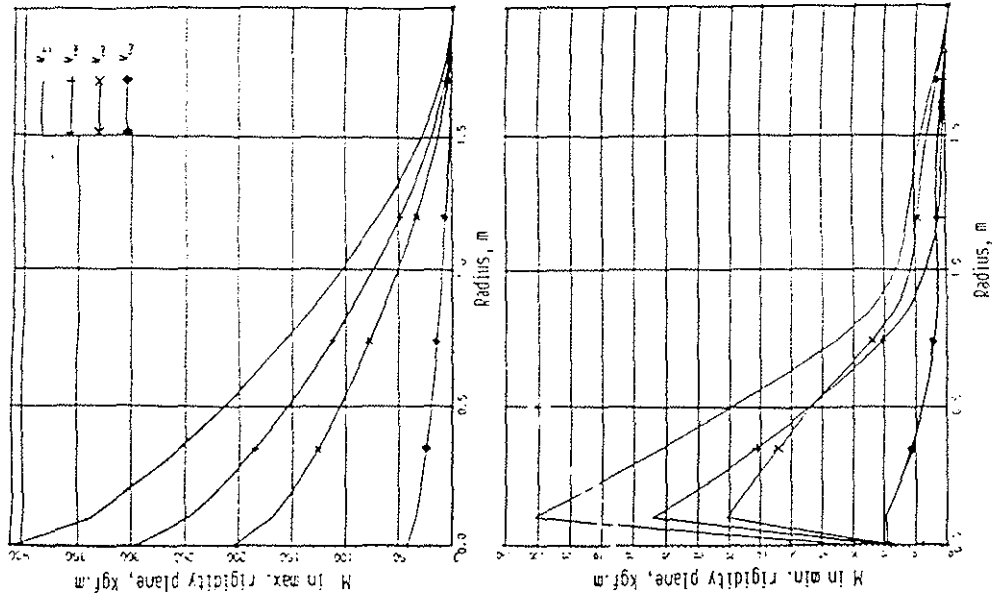


Figure 10. The Mi-8 gimbaled tail rotor blades.

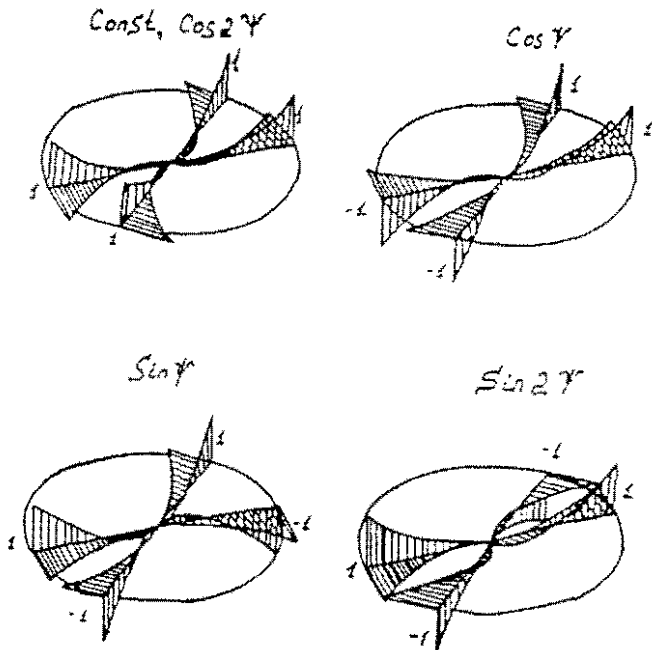


Figure 11. Normal oscillation modes of an X-form four-bladed tail rotor.

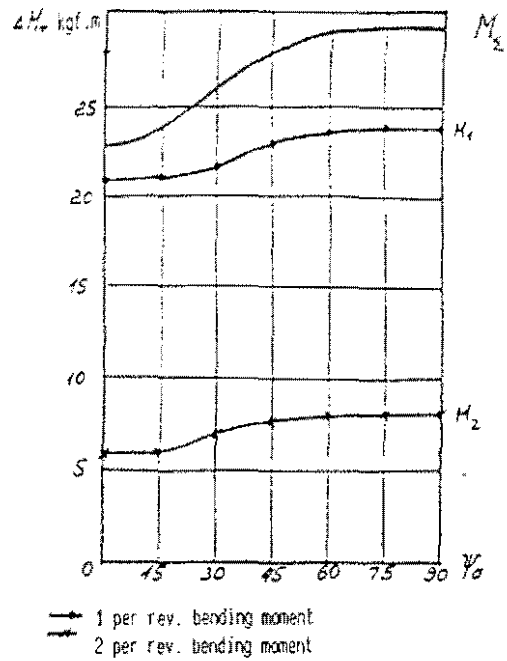


Figure 12. Blade out-of-plane bending moment versus azimuth of the blade pairs in the Mi-28 tail rotor.

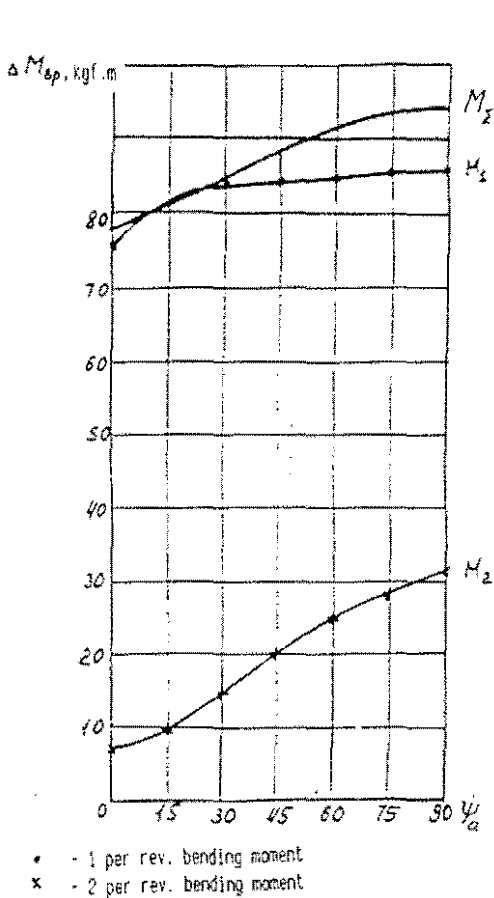


Figure 13. Blade in-plane bending moment versus azimuth of the blade pairs in the Mi-28 tail rotor.

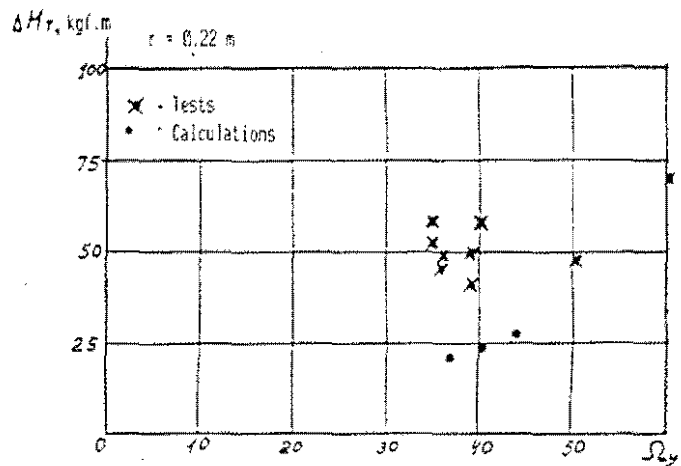


Figure 14. Variable out-of-plane blade bending moment for the Mi-28 tail rotor.

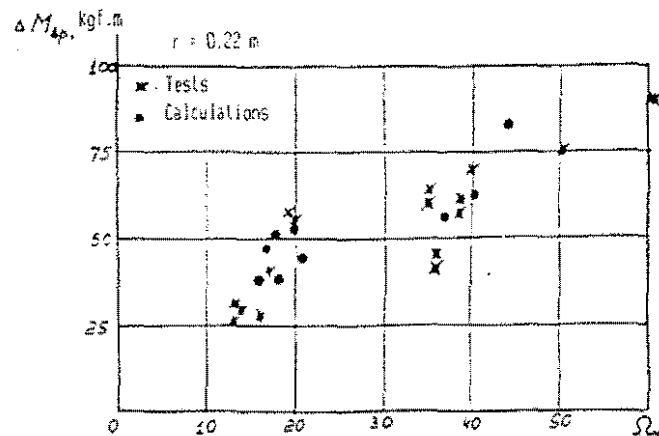


Figure 15. Variable in-plane blade bending moment for the Mi-28 tail rotor.